JET–P(98)46

V P Bhatnagar et al

Edge Localized Modes and Edge Pedestal in NBI and ICRF Heated H, D and T-Plasmas in JET

JET–P(98)46

Edge Localized Modes and Edge Pedestal in NBI and ICRF Heated H, D and T-Plasmas in JET

V P Bhatnagar, J Lingertat, R Barnsley, P Breger, J Christiansen, S Clement, J G Cordey, S Davies, J Ehrenberg, L-G Eriksson, G Fishpool, P Harbour, L Horton, H Jäckel, J Jacquinot, K Lawson, C Lowry, C Maggi, G Matthews, R Monk, D O'Brien, E Righi[1], G Saibene, R Sartori, B Schunke, A C C Sips, M Stamp, D F H Start, K Thomsen.

JET Joint Undertaking, Abingdon, Oxfordshire, OX14 3EA, UK.
[1]The NET Team, Max-Planck Institut für Plasmaphysik, Garching 85748, Germany.

Preprint of a Paper to be submitted for publication in Nuclear Fusion

December 1998

ABSTRACT

Based on experiments carried out in JET in D:T mixtures varying from 100:0 to 5:95 and those carried out in hydrogen plasmas, the isotopic mass dependence of ELM parameters and the edge pedestal pressure in neutral beam (NBI) and ion cyclotron resonance (ICRF) heated H-mode plasmas is presented. The ELM frequency is found to decrease with the atomic mass number both in ICRH and NBI discharges. However, the frequency in the case of ICRH is about 8 - 10 times higher than in the NBI case. Assuming that ELMs occur at a critical edge pressure gradient, limited by the ballooning instability, the scaling of the maximum edge pressure is most consistent with the assumption that the width of the transport barrier scales as the ion poloidal Larmor radius governed by the average energy of fast ions at the edge. The critical edge pressure in NBI heated discharges increases with the isotopic mass which is consistent with the higher deduced width of the edge transport barrier in tritium than in deuterium and hydrogen. The critical edge pressure in ICRH discharges is smaller, presumably, due to the smaller fast-ion contribution to the edge region. As a consequence of the edge pressure scaling with isotopic mass, the edge operational space in the n_e - T_e diagram increases with operation in tritium. If the evidence that the edge pedestal width is governed by the average energy of fast ions in the edge prevails, the pedestal in ITER would be controlled by the slowing down energy spectrum of α - particles in the edge.

1. INTRODUCTION

Edge localised modes (ELMs) [1,2] in a tokamak plasma are MHD instabilities which occur during H-modes [3] and produce bursts of energy and particles that are ejected through the separatrix to the scrape-off layer and ultimately end up in the divertor or on the first wall. These transient bursts can, in some cases, produce high peak heat loads [4-6] and severe erosion of the divertor target plates. This is a major issue for power and particle control in a reactor and makes the design of divertor target plates in ITER [7] a challenging task. ELMs are accompanied by spikes in the D_α-emission, the observation of which is now popularly considered as evidence of the presence of an H-mode. During an ELM, there is a rapid loss of energy and particles from the plasma and the stored energy is found to be reduced by a maximum of about 10% of its value before the ELM. In steady state, the stored energy recovers in between the ELM events. Despite these deleterious effects, it is desirable to operate ITER in an ELMy H-mode as this regime can provide sufficiently high confinement and, more importantly, it is beneficial in preventing the uncontrolled build up of density, impurities and helium ash. In order to optimize and off-set the losses against the gains, an understanding of the behavior of ELMs and their control is of paramount importance in providing an experimental basis for the satisfactory operation of ITER.

The H-mode is characterised by the formation of an edge transport barrier together with an improvement in the core confinement. The barrier creates a large pressure gradient close to the edge of the plasma which provides a pedestal for the rest of the profile. The energy stored in

an H-mode plasma can be considered to be constituted of two parts (i) the pedestal energy and (ii) the remainder which we term as the energy in the plasma 'core'. The turbulence in the core is found to scale as the gyro-radius similar to that expected from the gyro-Bohm transport model [8]. The pedestal energy is a significant part of the total stored energy [9] in neutral beam injection (NBI) heated discharges especially in ELM-free H-modes. The height and width of the pedestal can, in principle, be determined by the measurement of edge pressure profiles where a 'knee' in the profile is formed during H-modes. In this paper, we will investigate the scaling of the pressure on the top of the pedestal and assume that the large edge pressure gradient ∇p which develops over a region of width Δ is limited by a MHD instability. We will show that the pressure at the top of the pedestal scales as the ion poloidal Larmor radius ρ_L which is governed by the energy and mass of ions in the edge. A good knowledge of the scaling of the width and the height of the pedestal is important from the point of view of the prediction of the ITER edge operational space and energy confinement.

The theoretical understanding of the MHD physics of ELMs is at present incomplete and a number of models have been proposed to explain their occurrence. An excellent review of these models can be found in [2]. For the purpose of this paper, we confine ourselves to the idea that as a result of plasma heating leading up to the H-mode, the edge pressure gradient reaches a critical value ∇p^{crit} dictated by the ballooning stability limit [10-14]. This edge pressure gradient contributes significantly to the bootstrap current. Moreover, the increased edge temperature also causes a significant Ohmic current due to the increased conductivity of the plasma edge. As the growth rate of the low-toroidal mode number external kink mode (also the so-called peeling modes) increases with the edge current [15,16], this mode becomes unstable [2]. However, at high pressure gradients and at high edge currents, the ballooning and external kink instability limits tend to merge and it is not clear which instability actually triggers the ELM. After the ELM, the edge pressure gradient and the edge current are reduced, thus the plasma becomes stable and the cycle repeats itself. The rate of recovery and the ELM period are controlled mainly by plasma transport (see e.g. [17]).

The type of ELMs observed in a discharge depends on the plasma shape, the edge temperature and density, the proximity to the L-H transition, the edge pressure profile and MHD stability limits at the edge. Based on the experience of NBI discharges, an excellent discussion of the characteristics and classification of ELMs is given in [1]. It is believed that type I ELMs [1] are triggered when the plasma reaches the ideal Ballooning instability limit or by a low-n external kink mode. These ELMs feature a high pressure pedestal and the ELM frequency increases with power. However, type III ELMs [1] are believed to occur below the ideal instability limit and resistive ballooning modes may be implicated [2, 18]. These ELMs are associated with a low edge pedestal pressure, their frequency is higher and decreases with power ultimately transforming to type I ELMs at higher power [19].

For the same power flux crossing the separatrix, the edge pedestal in ICRH discharges is generally smaller but the energy confinement is similar to that with beams as the contribution of the core is more dominant due to more peaked power deposition profiles. The existence of a low pressure pedestal in ICRH discharges causes some of the ELM features to be markedly different from those of the NBI. The ELMs produced by ICRH have higher frequency and lower amplitude. The repetition rate and amplitude of ELMs is relatively less steady as compared to beams. However, other physical characteristics of ELMs, such as their dominant power dumping on the inner divertor leg, a sudden decrease in edge plasma parameters and a decrease in stored energy that are associated with ELMs are found to occur in both cases. But, in the case of ICRH, the perturbation of the above plasma parameters is typically 2-5 times smaller than with NBI [4].

Recently, JET has carried out experiments in DT plasmas [20,21] which were heated by NBI and ICRH. In these experiments, the isotope scaling of the H-mode threshold power, the energy confinement, ELM characteristics and the edge pedestal have been extensively studied as they constitute some of the most important issues to be resolved for a more accurate prediction of the ITER performance and the ignition margin. We note that the H-mode threshold power [19] is found to be independent of the heating method but ELMs and the pedestal characteristics do indeed depend on them. A detailed comparison of differences and similarities of ELMs and the pedestal in NBI and ICRH discharges has been presented elsewhere [22]. In this paper, we concentrate on the effects of isotopic mass on the parameters mentioned above. Experiments in D:T mixtures varying from 100:0 to 10:95 and those carried out in hydrogen plasmas permit us to study the effects of isotopic mass on the above parameters in a range extending from 1 to 3.

In section 2, we show JET experimental results on the pressure pedestal and on ELMs. After a brief discussion of the plasma configuration, parameters and general characteristics of ELMy H-mode discharges heated with NBI and ICRH, we present the isotopic mass dependence of ELM frequency both for ICRH and NBI discharges. We then discuss the edge operational diagram together with the influence of isotopic mass on different limiting boundaries. Subsequently we compare the experimental data with predictions of several different scaling laws in which the pedestal width is presumed to be related to the poloidal ion Larmor radius governed either by the thermal or the fast-ion energy in the edge. Experimental data on the edge electron pressure and its drop at an ELM are then presented followed by data on the scale length and the extent of electron temperature perturbations due to ELMs in H, D and T-plasmas. Finally, the plasma energy stored in the pedestal and its dependence on the isotopic mass are presented. The discussion and conclusions of the paper are in Section 3.

2. EXPERIMENTAL RESULTS

2.1 Plasma Parameters and Configuration.

For the experimental results presented here, we have selected ELMy H-mode discharges in hydrogen and deuterium-tritium D:T mixtures varying from 100:0 to 10:95. The main emphasis in this selection is to find representative discharges in H and D-T mixtures that have similar external parameters, plasma configuration and additional heating power. A detailed analysis of these discharges is then presented. For discharges heated by ICRH, after an extensive wall conditioning procedure, the working gas (H, D or T) or the required gas mixture is injected directly into the torus by a gas valve. For NBI heated discharges, the plasma mixture, in addition, is determined by the species used in the NB injectors. The injection energies for different species are: H°,120 keV; D°,140 keV or T°,155 keV. Generally, the configuration used in these experiments is JET divertor Mark IIAP [23], single-null X-point, low triangularity (δ~0.2) plasma. The discharges have been obtained at toroidal fields varying in a range of B_ϕ ~1-3 T and plasma currents I_P ~ 1-3 MA. For ICRH discharges, a central minority heating scheme with hydrogen as the minority species is applied. The 4-strap A2 ICRH antennae [24] are operated in dipole ($0\pi0\pi$) phasing. Standard JET diagnostics for electron density (n_e), electron temperature (T_e), and ion temperature (T_i) have been discussed elsewhere [25]. The tritium concentration is measured by neutron emission analysis, Balmer emission spectroscopy, partial pressure measurements in the sub-divertor volume and neutral particle analysis [26]. The electron temperature profile is measured by electron cyclotron emission and covers generally the outer half of the plasma minor radius. The ion temperature profile and ion density profile are obtained from active charge-exchange spectroscopy [27]. The number of interferometer channels measuring n_e is limited and the only channel covering the outer edge region is located at R = 3.75 m whereas the JET magnetic axis is at R_0 ~ 2.9 m and the horizontal minor radius is ~ 0.9 m. The plasma separatrix at midplane is generally located at around R = 3.81 - 3.86 m depending on the discharge selected. Due to the absence of density measurements further out in the edge, the exact location and form of the density pedestal, the edge pressure profile and the edge pressure gradient are unknown. Moreover, even with edge density profiles recently available at JET, the absolute spatial accuracy of the measured profile data would limit the evaluation of the pressure profile. The latter combines four measured profiles, where three of them (T_e, n_e, and T_i/n_i) have independent radial scales. The absolute spatial accuracy required for a reliable evaluation of the pressure gradient would be ~ 3 mm, or 0.08% of the major radius. In the absence of the required accuracy of measurements, we restrict ourselves to an investigation of the edge pedestal pressure at R = 3.75 m, though the pressure pedestal is presumed to be located at a somewhat larger radius. Calculated quantities, like the poloidal Larmor radius, are related to the same location at R = 3.75 m. In cases where the ion temperature data is not available, we discuss the results in terms of electron pressure p_e only, implicitly assuming that $p_i = p_e$. For NB heated discharges, the radial profile of the average energy of the fast particles is obtained from the CHEAP code

[27]. This code uses electron, ion and impurity density and temperature profiles as input data and then calculates the pressure and density profile of the fast particles by analytically treating the beam-target plasma interaction. The presence and onset of ELMs is generally detected by measuring $H\alpha/D\alpha/T\alpha$-line emission along a vertical chord.

2.2 General Characteristics of ELMy Discharges heated with NBI and ICRH.

As an illustration, we show time traces of two discharges additionally heated by NBI and ICRH in Figures 1 and 2 respectively, where the D:T plasma composition was 5:95. In the discharge heated by NBI (T°-beam power = 10 MW), the measured diamagnetic plasma stored energy reached 7 MJ. Without subtracting the fast ion energy, the energy confinement time normalized to the H-mode ITERH97-P [28] scaling was about 1.5 in the ELM-free phase for the first 2 s and then remained at ≥1 during the low frequency ELMs seen as spikes in the $D\alpha$-signal presented in the 5th box from top in Fig. 1. Central and edge (R=3.75m) electron temperatures are shown in box 3 where the sudden drops of T_{e0} indicate the occurrence of sawteeth. The central and edge (R=3.75m) line-averaged edge densities shown in box 4 indicate that in this H-mode tritium shot, the n_e-profile is very flat (see also Fig. 3).

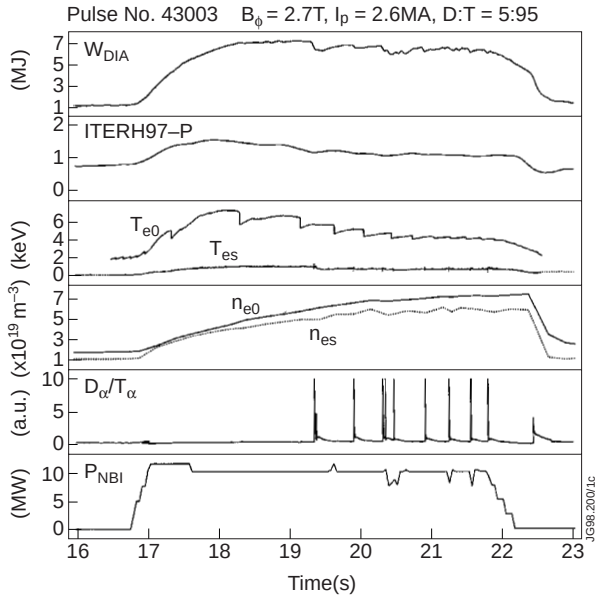

FIG. 1. Time traces of a neutral beam heated ELMy H-mode discharge in a 5:95 D:T mixture at a power level of ~10 MW at B_ϕ= 2.7 T and I_p=2.6 MA. Here, W_{DIA} represents the diamagnetic stored energy, ITERH97-P is the confinement enhancement factor over the ITER H-mode scaling [28], T_{e0}, T_{es}, n_{e0} and n_{es} indicate the central and edge electron temperatures and central and edge electron densities respectively, D_α/T_α represents the Balmer-α emission from the edge of the plasma indicating the presence of ELMs and ELM-free periods and P_{NBI} is the T°-neutral beam input power.

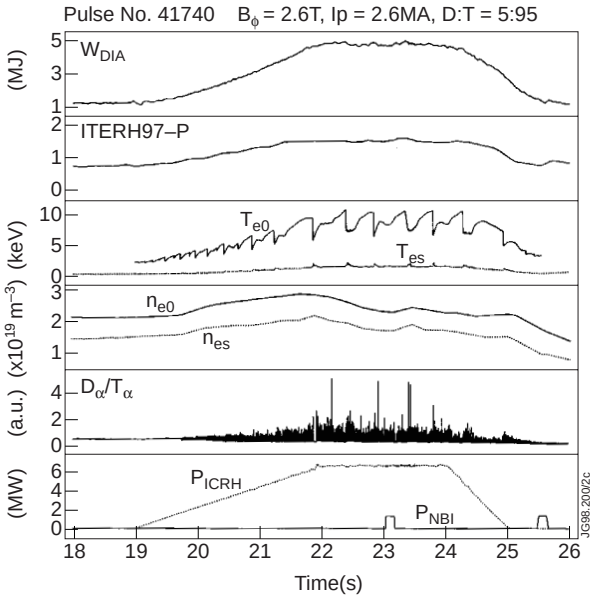

FIG. 2. Time traces of an ICRF heated ELMy H-mode discharge in a 5:95 D:T mixture at a power level of ~ 6.8 MW at B_ϕ= 2.6 T and I_p=2.6 MA. Here, P_{ICRH} is the ICRH input power at 42.5 MHz. For other symbols, see the caption of Fig. 1. The NBI power blips were used for ion temperature (T_i) diagnostic purposes.

The discharge shown in Fig. 2 is heated at a power level of 6.8 MW using the ICRH H-minority heating scheme in tritium plasma at a frequency of 42.3 MHz. The diamagnetic stored energy reached about 4.8 MJ and the ITERH97-P confinement factor without subtracting the fast ion energy is about 1.5. In this discharge, the calculation of the fast-ion energy fraction evaluated by the PION code [29] has large error bars and it is estimated to vary between 35-54% and the thermal H97 confinement factor is estimated to be 0.69-1. The central electron temperature (see box 3) rose to 10 keV as the H-minority fast ions relax predominantly on the background plasma electrons.

The power crossing the separatrix P_{SOL} is an important parameter influencing the ELM behavior. P_{SOL} can be deduced by subtracting from the input power P_{in}, the power radiated from the bulk P_{bulk} and, in the case of NBI, the power lost due to shine-through and charge-exchange. The latter generally has large error bars. In calculating the P_{SOL} in the steady-state part of the discharges shown in Figs. 1 and 2. we find that it is approximately equal in the two cases with a value ~7 MW. But, the frequency of ELMs (D_α-signal in box 5 in Fig. 2) is much higher with ICRH as compared to that with NBI. This difference is further confirmed [21] in ICRH and NBI discharges when the input power was equal, making P_{SOL} even smaller in the case of NBI.

On a detailed examination of ELMs with ICRH, it is found that not only the frequency is higher but also the repetition rate and amplitude of ELMs is relatively less steady (see below). In addition, the amplitude of ELMs (D_α-signal) with ICRH is generally smaller by a factor of about 5-10 as observed in a single shot with successive NBI and ICRH heating [4]. A fast 2-D infra-red camera has been used to measure the temperature evolution of divertor tiles [5] during ELMs in deuterium discharges. Illustrative examples showing a comparison of tile temperature evolution during ELMs with ICRH and NBI are given in [4]. Typically the peak tile temperature exceeds 1200°C with type I ELMs produced by NBI whereas with ICRH ELMs, it is less than 500°C .

The plasma density, temperature and pressure profiles of electrons measured by the LIDAR diagnostic are illustrated in Fig. 3 for three NBI heated discharges in hydrogen, deuterium and tritium (D:T=5:95) which have been used for isotopic comparison in this paper. The P_{in}-P_{bulk} for these discharges are 8.7, 9.5 and 7.3 MW respectively. The single null X-point plasma configuration in the three discharges is very similar to each other and the toroidal field (B_ϕ) and plasma current (I_p) values are 2.7T and 2.6MA respectively. The profiles in the case of hydrogen are time-averaged over 1 s whereas those for deuterium and tritium are averaged over 2 s. We note that the electron density profiles are rather flat in the main plasma especially those in deuterium and tritium plasmas. But, the density in the hydrogen discharge is lower by a factor of about 0.6 (see below). The electron temperature profiles are roughly about the same in the three shots. The corresponding electron pressure (p_e) profiles are shown in box 3 where it is seen that that p_e is the highest in tritium plasma and the lowest in hydrogen throughout the profile.

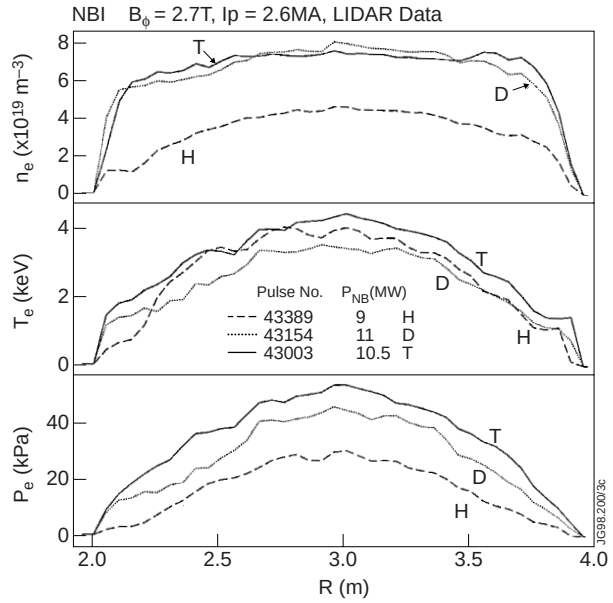

FIG. 3. Spatial profiles of electron density, temperature and pressure measured by the LIDAR diagnostic in three NBI shots made in hydrogen, deuterium and tritium plasmas at power levels indicated in the figure at B_ϕ= 2.7 T and I_p=2.6 MA. The profiles have been averaged over 1 s for H-plasma and 2 s for D and T-plasmas. The plasma center is at ~2.96 m.

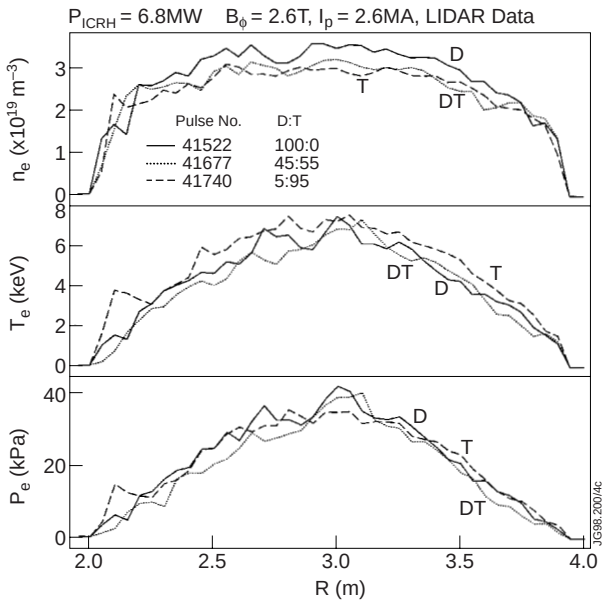

FIG. 4. Spatial profiles of electron density, temperature and pressure in three ICRH shots made in D:T mixtures of 100:0, 45:55 and 5:95 at B_ϕ= 2.6 T and I_p=2.6 MA. All the three profiles have been averaged over 1 s. See also the caption of Fig. 3.

A set of three ICRH discharges, similar to the ones with NBI discussed above, has been used for comparison in which the B_ϕ and I_p are 2.6T and 2.6 MA respectively. For these discharges, P_{in}-P_{bulk}=6.6 MW. Plasma profiles, averaged over 1 s, for these ICRH discharges in D:T mixtures of 100:0, 45:55 and 5:95 are shown in Fig. 4. We note that none of the parameters show a significant difference in the profiles of the three shots. However, the ELM frequency, though different in the three shots (see below), is about ten times higher than in the NBI cases and the electron pressure profile is more peaked due to the more peaked power deposition in the case of ICRH.

2.3 ELM frequency dependence on isotopic mass.

We compare the behavior of ELMs produced in NB (H, D and T-plasmas) and ICRF (D, D-T and T-plasmas) heated discharges as shown in Figs. 1 and 2 for studying the dependence of the ELM frequency on the isotopic mass. The D_α-signal is presented in Figs. 5 and 6 respectively for NBI and ICRH discharges having different isotope mixture. Power levels are as indicated in the figures. We note that, in the case of NBI heated discharges in tritium, after a very short period of transition ELMs at about 17 s (see box 3, Fig. 5), there is a long ELM-free period and then giant ELMs are produced saturating the T_α/D_α-signal. The frequency of these ELMs is relatively low. In the case of D-plasma (box 2), the initial ELM-free period is smaller than in the tritium discharge and once again giant ELMs are produced but their frequency is higher than in

the case of tritium. The frequency of ELMs is not completely steady and each ELM is accompanied by other associated ELMs making their occurrence a complex phenomenon. Note, however, that practically the same minimum level of the D_α-signal is achieved after each of these complex ELMs. In the case of hydrogen plasma (box 1), the initial period is partially filled by tiny ELMs and the subsequent ELMs have on average lower amplitude and significantly higher frequency.

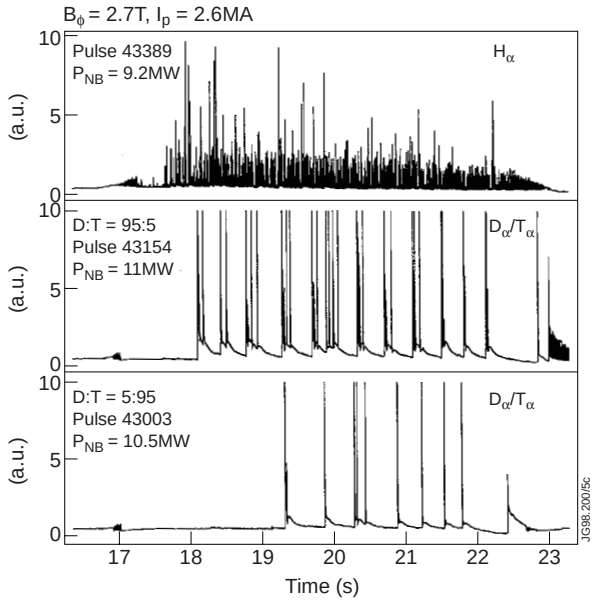

FIG. 5. Time traces of $H_\alpha/D_\alpha/T_\alpha$-signal for NBI heated discharges at B_ϕ= 2.7 T and I_p=2.6 MA showing the ELM behavior in hydrogen, deuterium and tritium plasmas. The ELM amplitude is on average smaller in hydrogen plasma. The frequency of ELMs decreases as one moves from H to D and T-plasmas.

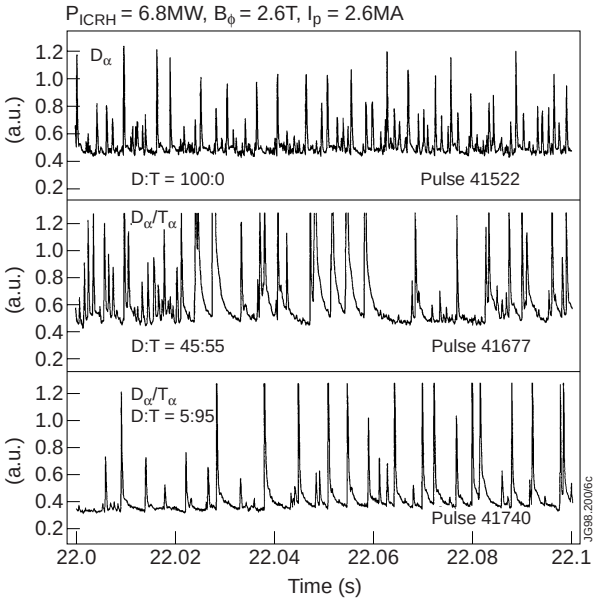

FIG. 6. Time traces of D_α/T_α-signal for ICRF heated discharges at B_ϕ= 2.6 T and I_p=2.6 MA showing the ELM behavior in D, DT and T-plasmas. The frequency of ELMs decreases as one moves from D to T-plasmas. Note that the time axis is 0.1 s whereas for ELMs in NBI discharges in Fig. 5 , it is 7 s.

Turning to the ELMs produced in ICRH discharges (see Fig. 6), we note that the frequency of ELMs is very high as seen by the scale of the time axis. The time behavior of ELMs varies from one ELM to the other and the frequency of ELMs decreases as one moves from D to T-plasmas. Note that during the time interval chosen for the display of D_α-signal in Fig. 6, the electron density is equal in the 3 discharges. At other time slices, the ELM frequency varied significantly but the frequency was on average smaller in tritium discharges than in deuterium. However, over the full duration of the discharge, the spread in frequency at each isotopic mass is large [21]. This is often caused by sawtooth crashes which lead to a heat wave that travels from the centre to the plasma edge and by increasing the edge pressure transiently is affecting the ELM frequency [4,22].

Based on the above measurements and those of other discharges, the ELM frequency is plotted, in Fig. 7, as a function of the isotopic mass both for NBI and ICRH discharges. In all cases considered, the input power was at least a factor of two higher than the H-mode power threshold manifested by the appearance of the transition ELMs. Note that in NBI and ICRH

discharges, the ELM frequency decreases as the isotopic mass of the plasma mixture is increased. However, the frequency of ELMs in the case of ICRH discharges (see right-hand scale) is about a factor of 10 higher than in NBI discharges. As we will discuss below, this may be related to the width of the edge pedestal and the level that the edge pressure can attain before an ELM is triggered.

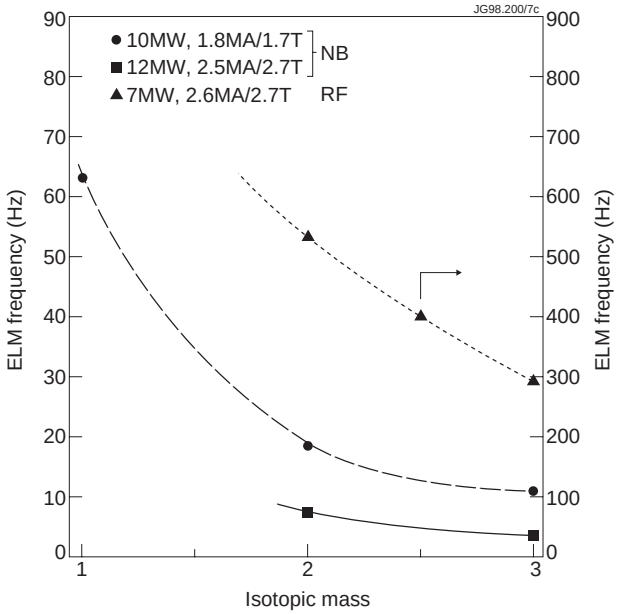

FIG. 7. ELM frequency as a function of isotopic mass of plasma species in ICRH and NBI heated discharges. The right-hand scale corresponds to the ICRH data.

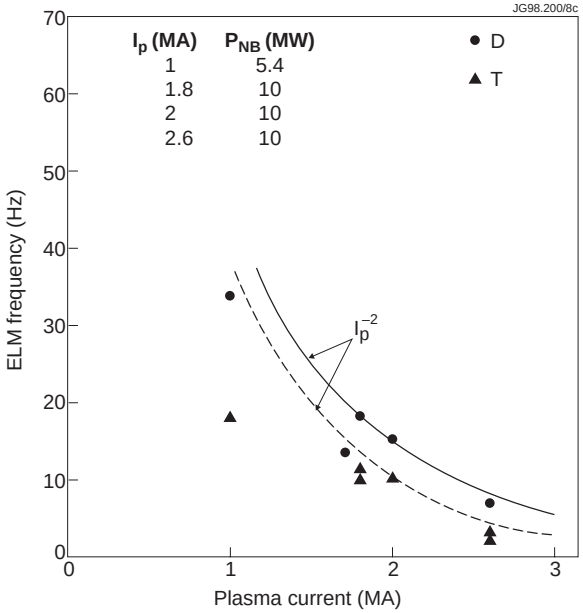

FIG. 8. ELM frequency as a function of discharge current in D and T-plasmas in NBI heated discharges. The NBI heating powers are as indicated. The lines represent a I_p^{-2} dependence (normalised to a point) of ELM frequency.

Based on neutral beam heated discharges, we also plot, in Fig. 8, the ELM frequency as a function of plasma current in deuterium and tritium discharges. The power level is indicated in the figure. The toroidal field is increased in the same proportion as the plasma current (e.g. 1T/1MA, 2T/2MA and so on) to maintain the same safety factor q. We find that the ELM frequency decreases as the plasma current is increased. This is for discharges in deuterium fairly consistent with a theoretical model [30,31] where the ELM frequency is predicted to decrease as the square of the plasma current (see also [2]), whereas for the tritium case the decrease of ELM frequency with plasma current is much weaker.

2.4 Effect of isotopic mass on the edge operational space.

It is well known that the H-mode performance depends sensitively on the plasma edge parameters. The edge operational or n_e-T_e diagram [32-37] is a convenient way of characterizing the different operational regimes and events associated with the an H-mode discharge. These regimes have been identified as (i) L to H mode transition and transition ELMs, (ii) ELM-free H-mode (iii) Type I ELMs, (iv) Type III ELMs and (v) MARFE events (see e.g. Ref. [33]). The above diagram is constructed by plotting the measured edge electron temperature T_{es} and the

edge electron density n_{es} at a location in the plasma edge (close to but inside the separatrix) or if the resolution and extent of the diagnostics permit, at the top of the pressure pedestal. In JET, the above two parameters are taken at R=3.75m, as described in Section 2.1. Such a diagram for JET ICRH and NBI heated discharges is shown in Fig. 9. As the input power is increased above the L-H threshold value, the transition from L to H-mode takes place [19], at relatively low T_{es} and n_{es} values (see Fig. 9). This is accompanied by the occurrence of small ELMs the so-called transition ELMs. These transition ELMs, according to the common classification scheme [1], are similar to type III ELMs. However, they have specific features which distinguish them from type III ELMs obtained in JET by strong gas puffing or impurity seeding. As the edge temperature and density are increased further, the H-mode discharge usually evolves into a non stationary ELM-free phase followed by type I ELMs. At higher densities or with impurity seeding, the discharge goes into the regime of type III ELMs. At very high gas puff rates, the edge temperature decreases below the value required for the L-H transition and the discharge ultimately falls back to the L-mode and finally disrupts after reaching the MARFE [10,23,38] limit.

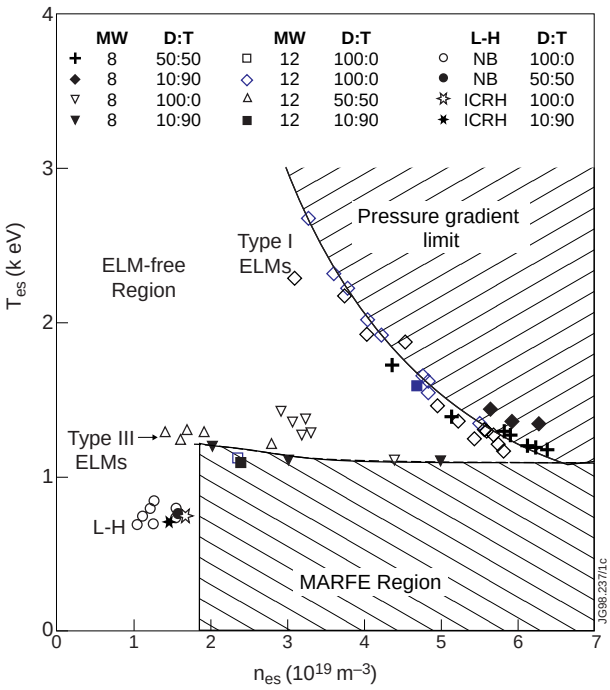

FIG. 9. Edge operational diagram in T_{es}-n_{es} plane showing the JET experimental data of Type I ELMs in NBI heated D-plasmas at 12 MW of input power. The 8 MW data points in D-plasma (inverted open triangles) do not reach the type I ELM boundary whereas in 50:50 and 10:90 DT mixtures, type I ELMs are obtained at this power as shown. The open and solid circles/stars show the location of L-H transitions in this diagram under different conditions as indicated.

At high edge temperature, it is assumed that the edge pressure gradient is limited by the ideal ballooning mode instability which, possibly on coupling to an external low-n kink mode, triggers a type I ELM. In Fig. 9, we plot an experimentally fitted boundary for type I ELMs (the solid line) for typical JET discharges at B_ϕ /Ip = 2.7T/2.6MA in D-plasma at a NBI power level of 12 MW. The shaded area limited by the solid line is assumed to be inaccessible for the discharge. In addition, a variety of experimental edge density and temperature data obtained at 2.6T/2.6MA in JET ELMy H-mode D-T discharges with ICRH and NBI heating at different power levels are plotted in Fig. 9. Open diamond symbols represent the data obtained with type I ELMs at 12 MW of NBI power in deuterium discharges. Bold plus and solid diamond symbols show the corresponding data in 50:50 and 10:90 D:T discharges representing approximately the isotopic mass of 2.5 and 3 respectively . These data lie beyond the ballooning stability boundary for deuterium discharges, and encroach into the shaded area, indicating that a higher edge pres-

sure can be reached in tritium discharges. The above observation of higher p_e in tritium discharges is consistent with the argument that type I ELMs occur at a fixed ∇p_e^{crit} provided the width of the edge pedestal increases with mass of the plasma ion species. The L-H mode threshold points shown (in the lower left-hand corner) show no marked difference either between ICRH and NBI data or D and T data [19]. The region of existence of type III ELMs is located around the nearly horizontal broken line in Fig. 9 and there seems to be no significant difference between deuterium and tritium discharges.

2.5 Scaling of the critical edge pedestal pressure

In the previous section we assumed that the edge pressure gradient is limited by its critical value for the ideal ballooning instability. In general the calculation of this limit is complex [10,12] and its determination in a real tokamak geometry requires quite involved numerical computations [16]. But, in the case of a large aspect ratio tokamak with circular flux surfaces, these calculations are relatively straightforward. Commonly, the stability limit is presented in a s-α diagram where the magnetic shear s in a tokamak geometry is defined as $s= (r/q)\nabla q$ and $\alpha = - (2\mu_0 R q^2/ B_\phi^2) \nabla p_{crit}$ is a measure of the pressure gradient responsible for the ballooning instability. Further, $\nabla q \equiv dq/dr$, $\nabla p \equiv dp/dr$, μ_0 is the vacuum permeability, q is the tokamak safety factor, R is the major radius and B_ϕ is the toroidal field. Based on numerical computations, it has been found that in a significant range of the s-α stability diagram, the relationship is linear. Thus, a very simple model can be analyzed in which $\alpha \propto s$. However, for elongated and triangular plasmas this linear relationship is not valid. Analytical calculations show that α depends stronger than linear on s [39,40]. We will use the simple approximation $\alpha \propto s^\gamma$, where $\gamma > 1$. Furthermore, for reasons discussed in section 2.1, we approximate ∇p^{crit} by p^{crit}/Δ. In this way, we define the width Δ of the pressure pedestal or transport barrier. Using the definition of q and grouping the geometrical factors in the constant of proportionality, we obtain

$$p^{crit} \propto I_p^2 \bullet s^\gamma \bullet \Delta. \qquad (1)$$

By measuring the critical pressure p^{crit} and plotting it in the n_e-T_e diagram we can test different models describing the dependence of the pedestal width on plasma edge parameters. A common model assumes that a radial electric field develops in the edge region and suppresses, due to sheared rotation, the fluctuation driven transport in the transport barrier. The width of this region is related to the region of charge separation due to loss of ions, which is of the order of the poloidal Larmor radius ρ_L [41]. From there, the ansatz $\Delta \propto (AT)^{1/2}/I_p$ follows, where A is the ion mass number and T is either the ion temperature T_i or the averaged energy of the fast ion component E_{fast}. More refined models assume $\Delta \propto (a\rho_L)^{1/2}$ or $\Delta \propto a^{1/3}\rho_L^{2/3}$ [36,42]. Other approaches associate the charge separation to the penetration depth of neutrals into the edge plasma, which gives $\Delta \propto T_e^{1/2}/n_e$ [43] or simply assume Δ = constant.

In Fig. 10 we plot, for a series of NBI heated discharges in D plasma in which only the gas feed was varied (0 to 3.5×10^{22} s^{-1}) and which remained mainly in the type I ELM regime, the

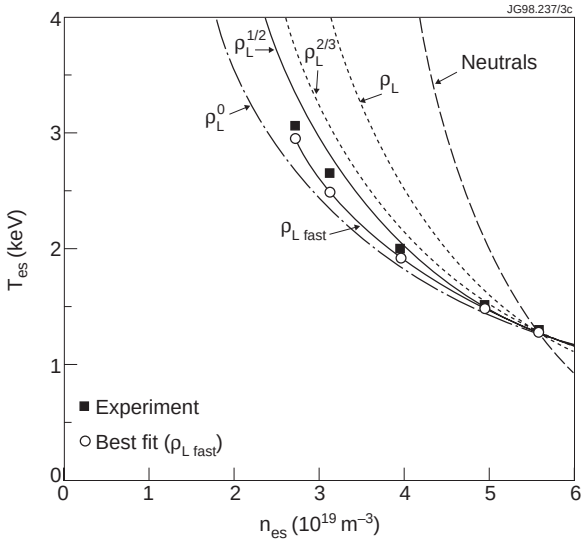

FIG. 10. Experimental T_{es}, n_{es} data (squares) of type I ELMs along the pressure gradient ballooning instability limit at 12 MW in D-plasmas is compared with several models of the width of the edge pedestal. The pedestal width is assumed to be equal to a power of the ion poloidal Larmor radius (ρ_L) determined by the thermal ions or the fast-ion averaged energy in the edge (ρ_{Lfast}). Neutral refers to a pedestal width scaling governed by the ionization length of neutrals.

measured values of $p_e^{crit} = n_e^{crit} T_e^{crit}$ in an n_e-T_e diagram together with curves derived from different assumptions on Δ discussed above. All curves are normalised to the measured p_e^{crit} at $n_e = 5.6\times10^{19}$ m^{-3}. The solid line connecting open circles represents the calculated values when Δ is assumed to scale as $\Delta \propto \rho_L(E_{fast})$. The best agreement between data points and model curves is achieved for the cases $\Delta \propto \rho_L(E_{fast})$ and $\Delta \propto \rho_L(T_i)^{1/2}$.

The scaling of the edge pedestal pressure is further evaluated for a number of NB heated JET discharges in which the safety factor q is held constant but B_ϕ and I_p are varied in a range of 1.7-2.9 T and 1.7-2.9 MA respectively. Also, the value of magnetic shear s at the edge is varied between 2.9 to 4 and the ion mass number between 1 to 3. These discharges were obtained without external gas fueling. The total edge pressure just before the occurrence of ELMs is then compared against the total pressure calculated using Eq. (1) with different assumptions on Δ as discussed above. For illustration, we show the two best fits out of six used for comparison, one with ρ_{Lfast} and the other with $\rho_{Lthermal}$ in Figs. 11 and 12 respectively. The squares in these two figures refer to the data taken at the maximum pressure before selected ELMs and triangles refer to an averaged pressure before all ELMs. For good agreement, the data should lie on a straight line. Among these two, it is seen that the scaling based on the ion poloidal Larmor radius determined by the fast ions in the edge (ρ_{Lfast}) gives the best fit. The average energy of the fast ions E_{fast} at R = 3.75 m was calculated by using the CHEAP code (see section 2.1), which delivers for the discharges used in Figs. 11 and 12 an energy range of 11.2 - 88.4 keV.

The same scaling with ρ_{Lfast} has been obtained for hot-ion H-mode discharges [44]. However, two other scaling attempts which include in the data set gas fuelled discharges find a better correlation with $\rho_{Lthermal}$ [45,46]. Whether this difference is caused by gas fuelling alone is currently under investigation.

We determined the exponent γ in Eq. (1) by testing the quality of the fit for γ = 1, 1.5, 2, 2.5 and 3. This test gave the best result for γ = 2. However, the values for s_{95} are calculated by the equilibrium reconstruction code EFIT without taking the bootstrap current into account. Therefore, a prudent approach gives $\gamma > 1$ as the result of this fitting procedure. Using full MHD calculations for a different set of JET discharges shows that indeed $\alpha \propto s^\gamma$ with $\gamma > 1$ [47].

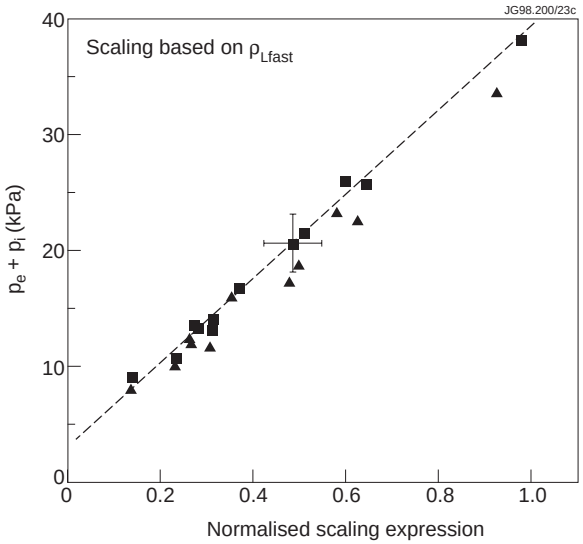

FIG. 11. Experimental data of total (electron and ion) edge pedestal pressure (symbols) is plotted against the normalized expression $I_p s^2 (A<E>_{fast})^{1/2}$ based on the fast-ion averaged energy in the edge. The squares and triangles refer respectively to peak and average values of several ELMs studied in a discharge.

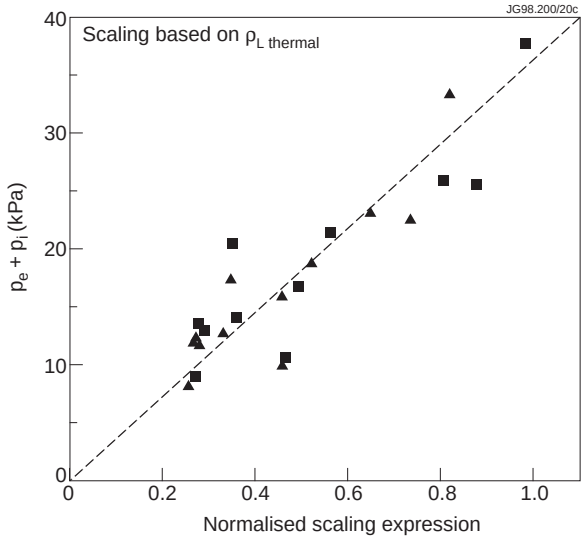

FIG. 12. Experimental data of total (electron and ion) edge pedestal pressure (symbols) is plotted against the normalized expression $I_p s^2 (A<E>_{thermal})^{1/2}$ based on the thermal ion temperature in the edge. See the caption of Fig. 11.

2.6 Behavior of the edge electron pressure during an ELM.

As mentioned before, we have assumed that at the occurrence of an ELM, the critical edge electron pressure gradient ∇p_e^{crit} is limited by the ballooning instability. For a fixed ∇p_e^{crit}, a Δ increasing with increasing isotopic mass implies that a higher edge pressure can be achieved in tritium than in hydrogen discharges. Time traces of the edge electron pressure at R=3.75m are shown in Fig. 13 for three discharges heated by NBI in hydrogen, deuterium and tritium plasmas. The sudden drop of pressure in D and T-discharges shown coincides with the occurrence of ELMs as observed in the D_α-signal (see also Fig. 1). In the case of the hydrogen discharge, the frequency of ELMs is relatively high and the drop in pressure per ELM is much smaller. Note that the edge electron pressure is quite low in the hydrogen plasma and it increases as we change to deuterium and then to tritium plasmas. A similar dependence can be inferred if we consider the drop of pressure at each ELM.

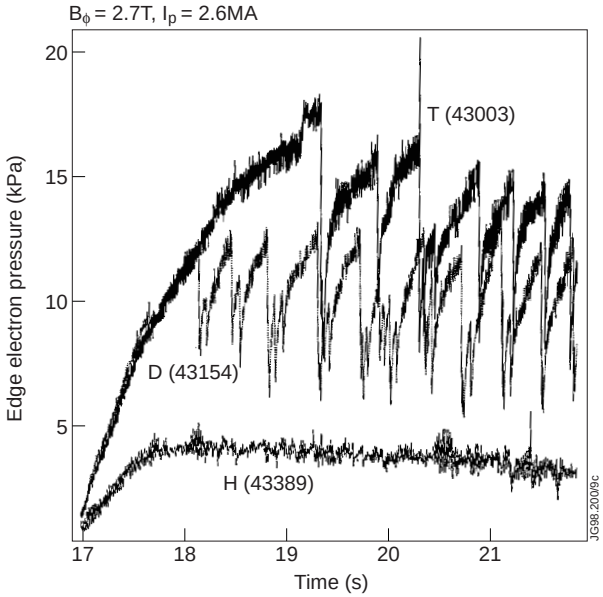

FIG. 13. Time traces of edge electron pressure for three NBI heated discharges in hydrogen, deuterium and tritium plasmas at B_ϕ= 2.7 T and I_p=2.6 MA showing the pressure drop at the occurrence of ELMs.

Figures 14 and 15 show the edge electron pressure before the start of an ELM and its drop during an ELM, respectively, for several ELMs in the H, D and T- discharges shown in Fig. 13. The broken lines represent the average for the number of ELMs considered. As mentioned above, the edge electron pressure clearly increases with increasing isotopic mass. Additionally, Fig. 14 shows the averaged edge electron pressure for ICRH discharges in D, 50:50 DT and T-plasmas without identifying specific ELMs.

The drop in edge electron pressure increases strongly with increasing isotopic mass in NBI heated discharges. In ICRF discharges, these drops are found to be much smaller and usually within the measurement noise.

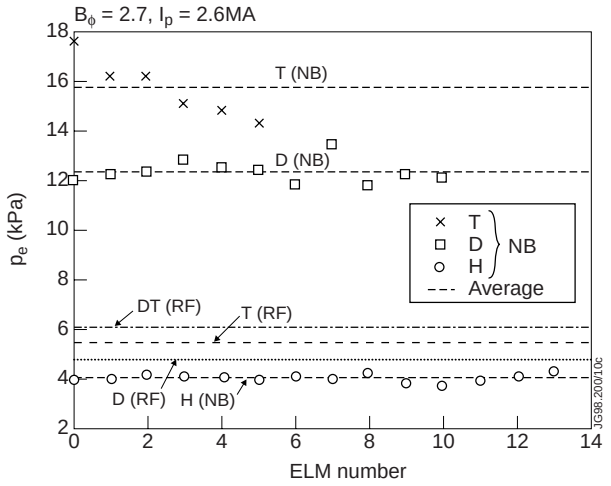

FIG. 14. Edge electron pressure (symbols) and mean value (broken line) for several ELMs in three NBI and three ICRF heated discharges in hydrogen, deuterium and tritium plasmas at B_ϕ= 2.7 T and I_p=2.6 MA.

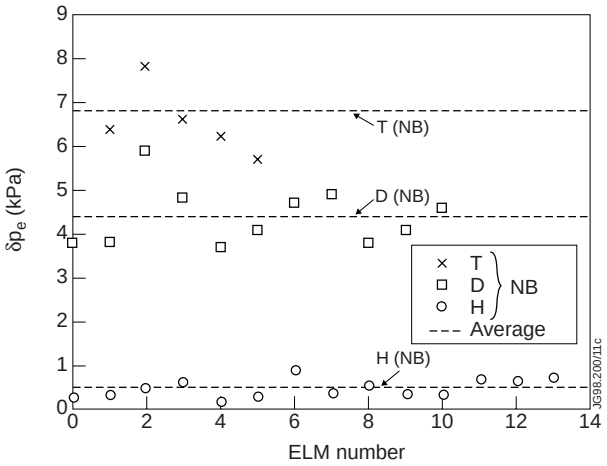

FIG. 15. Drop in edge electron pressure (symbols) and mean value (broken line) for several ELMs in the three NBI heated discharges in hydrogen, deuterium and tritium plasmas of Fig. 14.

2.7 Isotopic mass scaling of the edge electron pressure during ELMs.

Edge electron pressures for the above series of shots heated by NBI and ICRH are presented in Fig. 16 as a function of isotope mass for H, D, DT and T-plasmas. The data are normalised to the case I_p = 1.8 MA using the relation $\nabla p^{crit} \propto I_p^2$. From Fig. 16, we note that for NBI heated discharges, p_e^{crit} increases with the isotope mass whereas in the ICRH case, the edge electron pressure is not only significantly smaller but it is practically independent of the isotopic mass.

During NBI heating, beam neutrals that do not penetrate to the plasma core create a population of energetic ions near the edge. If, as discussed in section 2.5, the transport barrier width is determined by the poloidal ion Larmor radius of the energetic ions, then for a given pressure gradient limit the edge electron pressure increases with increasing atomic mass of the injected species ($p^{crit} \propto \sqrt{A}$).

In the case of ICRH there is no direct fast-ion deposition at the edge. The pedestal width is expected to be smaller which results in a smaller edge electron pressure compared to NBI discharges. Despite the lower edge pedestal with ICRH, the steady-state total stored energy in both ICRH and NBI cases is the same. This is due to the fact that the power deposition profile with

ICRH is more peaked than in the NBI case [22]. A TRANSP analysis carried out on two comparable ICRH and NBI discharges shows that the effective diffusivities (χ_{eff}) are similar.

With NBI heating, the fast particle species changes when the beam species is changed from hydrogen to deuterium or tritium. In the case of ICRH discharges, the heated species is hydrogen and it is independent of the background gas. Therefore, no dependence of the p_e^{crit} on the isotope mass of the background gas is expected. An increased edge pedestal is also found in ICRH discharges with -90° phasing resulting from the significantly broader fast-ion pressure profile due to wave induced particle drift outwards [22, 48].

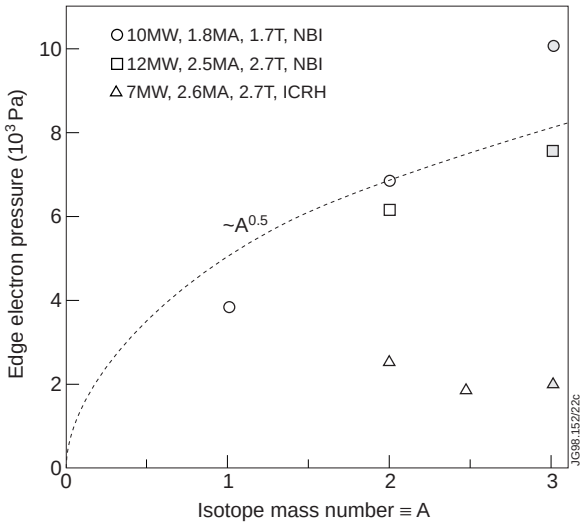

FIG. 16. Maximum edge electron pressure (@ R=3.75m in JET) is plotted as a function of isotopic mass in experiments carried out in different gas mixtures: hydrogen, deuterium, 50:50 D:T and 10:90 DT both in ICRH and NBI heated discharges. For comparison, the values have been normalized to Ip=1.8 MA using $\nabla p^{crit} \propto I_p^2$.

2.8 Isotopic mass dependence of the electron temperature perturbation during an ELM.

At the occurrence of an ELM, particles are ejected from the plasma and there is a drop in temperature and density at the plasma edge. The perturbation in the electron temperature is generally found to be highest in the type I ELM regime. In Fig. 17, we present the ECE measured electron temperature drop as a function of major radius in a semi-log plot for NBI heated discharges in hydrogen, deuterium and tritium plasmas where the maximum of δT_e has been taken in a time interval of $\delta t < 1$ ms after an ELM. The ECE data further into the edge are unreliable due to non blackbody radiation and are not shown. We note that the scale length of the amplitude drop is smallest in hydrogen plasma and increases as one goes from hydrogen to deuterium and tritium plasmas. Associating this scale length with the transport barrier width Δ shows its increase with isotope mass as expected from the assumed scalings of Δ with the poloidal Larmor radius.

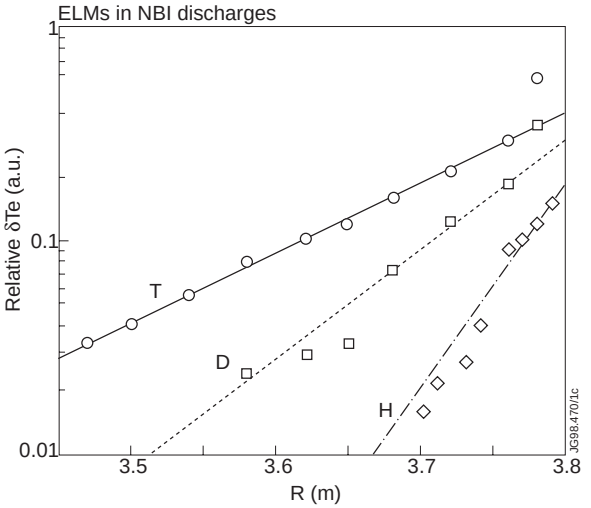

FIG. 17. Relative drop in electron temperature at the occurrence of ELMs is plotted as a function of major radius in a semi-log plot for NBI heated discharges in hydrogen, deuterium and tritium plasmas. The lines shown are for guidance of the eye only. The slope shows qualitatively the scale lengths of the affected plasma region by an ELM.

2.9 Pedestal stored energy dependence on isotopic mass..

The stored energy in H-mode discharges can be considered to be composed of two parts: (i) core and (ii) the pedestal. We write

$$W_{tot} = W_{core} + W_{ped}$$

where W_{ped} is obtained by integrating the pedestal pressure from the centre to the edge and W_{core} is obtained by subtracting W_{ped} from the total stored energy. Detailed confinement analysis based on JET discharges has been carried out in Ref. [9] and it has been found that the (a) the core is governed by gyro-Bohm transport ($\sim A^{-0.2}$) and (b) the pedestal energy in the ELMy H-mode scales as $\sim A^{0.5\pm 0.2}$. For the global energy confinement, the two mass dependencies nearly cancel each other resulting in a very weak mass dependence. In Fig. 18, we show the kinetic energy stored in the pedestal, for two sets of discharges (a) B_ϕ /Ip = 1.8T/1.8MA and (b) 2.7T/ 2.6MA in H, D and T-plasmas where in the first set, the NBI power input was 10 MW and in the second set it was 10.5 MW except in the case of hydrogen discharge for which it was 9.5 MW. The pedestal energy is calculated by using the edge pressure obtained at R=3.75m and multiplying it with the plasma volume integrated from the centre to that radius. In this calculation, we make an error of about 5% as we have neglected the volume beyond R=3.75 m. We find that the pedestal energy increases with the isotopic mass and is qualitatively consistent with the scaling presented in Ref. [9].

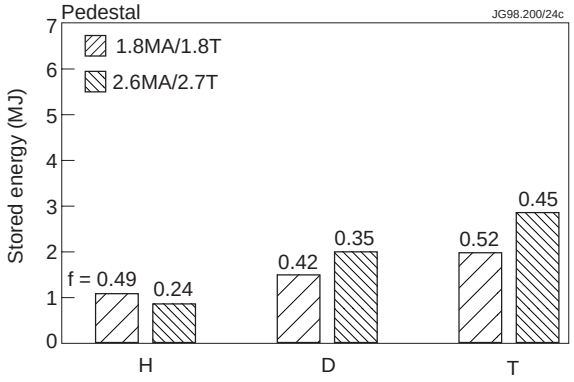

FIG. 18. Plasma stored energy in the edge pedestal is plotted as a function of isotopic mass in NBI heated discharges at B_ϕ= 2.7 T/ I_p=2.6 MA and B_ϕ= 1.8 T/ I_p=1.8 MA. The values of f represent the fraction of pedestal energy to the total energy.

3. DISCUSSION AND CONCLUSIONS

In this paper, we have presented experimental results on edge localized modes (ELMs) and on the edge pedestal observed in H-mode discharges in JET. The experiments have been carried out in single null X-point plasmas in hydrogen and in D:T mixtures varying from 100:0 to 5:95. The main auxiliary heating methods used are NBI and ICRH. We have concentrated on the isotopic mass dependence of ELM characteristics such as frequency, drop in edge pressure and the spatial extent of the electron temperature perturbation at the occurrence of ELMs. Also, the mass dependence of the critical edge plasma pressure has been investigated. A comparison of differences and similarities of ELMs and of the edge pedestal in ICRH and NBI heated plasmas is discussed elsewhere [22].

A number of theoretical models have been proposed to explain the occurrence and characteristics of ELMs [2]. Since ELMs are accompanied by bursts of MHD activity, ideal and resistive ballooning modes, external kink modes and ‘peeling’ modes have been put forward as the

underlying basis for the occurrence of ELMs. Also, limit cycle solutions of the transport equation governing the plasma edge region have been used which e.g. involve sheared rotational stabilization. In other theories, elements of both of the above have been combined with MHD or pressure driven fluctuation transport. For the purpose of this paper, we have confined ourselves to the idea that in H-modes, the edge pressure gradient reaches a critical value ∇p^{crit} determined by the ballooning stability limit $\nabla p^{crit} \propto I_p^2 .s^{\gamma}$ where I_p is the plasma current, s is the edge magnetic shear and $\gamma > 1$. An ELM is accompanied by a drop in the edge pressure gradient. The edge plasma then becomes stable and the cycle repeats itself. The rate of rise of pressure (or the recovery) and the period of the cycle depends mainly on the plasma transport.

Furthermore, we have assumed that the critical edge pressure gradient ∇p^{crit} can be simplified by $\nabla p^{crit} = p^{crit}/\Delta$, where p^{crit} is the critical pressure at the top of the pedestal and Δ the pedestal width and that by analysing the scaling of p^{crit} we find the scaling of the pedestal width Δ. In principle, one should be able to measure the edge pressure gradient and the width of the pressure pedestal, but due a lack of spatial resolution and accuracy of edge diagnostics, no such measurements are available at JET. The scaling found for the critical edge pressure is most consistent with the assumption that the pedestal width is proportional to the ion Larmor radius and the Larmor radius in turn is controlled by the fast ion population in the plasma edge. This result was obtained for NB heated discharges without external gas fueling.

These findings seem to be consistent with the low edge pressure observed in ICRH discharges with central plasma heating schemes in which there is no direct fast ion energy deposition in the edge. In fact, by deliberately depositing ICRH power at the edge by mixed central and off-axis heating, it was possible to increase the critical edge pressure. The higher the critical edge pressure, the larger is the drop in edge pressure at the occurrence of an ELM. The ELM frequency also decreases as the critical edge pressure becomes higher since during the ELM recovery cycle, more time elapses before the pressure reaches its critical value. This is consistent with the experimental fact that the ELM frequency in routine ICRH discharges is a factor of 8-10 higher than in the NBI discharges. Similar behavior is also found in NBI discharges in hydrogen where the edge pressure is low and the ELM frequency is higher.

In conclusion, the ELM frequency is found to decrease with isotope mass both in ICRH and NBI discharges. But, the frequency in the case of ICRH is about 8-10 times higher than the NBI case. This has a favorable consequence for ITER concerning the peak heat load on the divertor plates which in JET is smaller by a factor of 2-5 in the case of ICRH as compared to NBI. The pedestal width scaling presented here is different from that assumed in the ITER Final Design Report [49]. If the evidence that the edge pedestal width is governed by the averaged energy of fast ions in the edge prevails, the edge pedestal pressure during ignited regimes in ITER would be dictated by the slowing down energy spectrum of α-particles. Further dedicated experiments are planned to verify the reported scaling.

ACKNOWLEDGEMENTS.

Contributions of the JET tokamak operation team, the NBI and ICRH plant teams, the AGHS group and those operating the diagnostics used in the experiments reported here are gratefully acknowledged.

REFERENCES

[1] ZOHM, H., Plasma Physics Controlled Fusion, 38 (1996) 105.

[2] CONNOR, J. W., Plasma Physics Controlled Fusion, 40 (1998) 191.

[3] WAGNER, F. et al., Phys. Rev. Letters, 49 (1982) 1408.

[4] BHATNAGAR, V.P. et al., in Controlled Fusion and Plasma Physics (Proc. 24th Eur. Conf, Berchtesgaden, 1997), vol.21A, Part I, European Physical Society, Geneva (1997) 77.

[5] GAUTHIER, E. et al., in Controlled Fusion and Plasma Physics (Proc. 24th Eur. Conf, Berchtesgaden, 1997), vol.21A, Part I, European Physical Society, Geneva (1997) 61

[6] CLEMENT, S et al., "Power Deposition in the JET Divertor during ELMs" Proc. 13th International Conf. on Plasma Physics Surface Interaction in Controlled Fusion Devices, San Diego, May 1998, to be published in J. Nucl. Materials.

[7] AYMAR, R., et al., ITER JOINT CENTRAL TEAM, HOME TEAMS, in Fusion Energy (Proc.16th Int. Conf. Montreal, 1996), vol.1, IAEA, Vienna (1997) 3.

[8] PETTY, C.C., LUCE, T.C., in Controlled Fusion and Plasma Physics (Proc. 24th Eur. Conf, Berchtesgaden, 1997), vol.21A, Part III, European Physical Society, Geneva (1997) 1085.

[9] CORDEY, J.G. et al., 'Plasma Confinement in JET H-mode Plasmas with H, D, D-T and T Isotopes', Submitted for publication to Nucl. Fusion special issue.

[10] WESSON, J., 'Tokamaks', Clarendon Press, Oxford, 2nd edition, 1997.

[11] DOBROTT, D. et al, Phys. Rev. Lett., 39 (1977) 943.

[12] CONNOR, J.W. et al, Phys. Rev. Lett., 40 (1978) 396.

[13] GOHIL, P. et al., Phys. Rev. Lett., 61 (1988) 1603

[14] IGITKHANOV, Yu. Et al., in Controlled Fusion and Plasma Physics (Proc. 24th Eur. Conf, Berchtesgaden, 1997), vol.21A, Part III, European Physical Society, Geneva (1997) 989.

[15] HUYSMANS, G.T.A. et al., in Controlled Fusion and Plasma Physics (Proc. 22nd Eur. Conf, Bournemouth, 1995), vol.19C, Part I, European Physical Society, Geneva (1995) 201.

[16] HUYSMANS, G.T.A. et al., Nucl. Fusion 38 (1998) 179.

[17] TARONI, A. et al., Contribution To Plasma Physics 38 (1998) 37.

[18] CHANKIN, A.V., SAIBENE, G., 'Interpretation of the H-mode Operational Diagram through Similarity Parameters for Edge Transport Mechanisms', Report JET-P(98)22, JET Joint Undertaking, Abingdon, (UK). Submitted to Plasma Phys. Contr. Fusion.

[19] RIGHI, E. et al., 'Isotope Scaling of the H-mode Power Threshold in Tritium, Deuterium

and Hydrogen Plasmas on JET', Submitted for publication in Nucl. Fusion special issue.
[20] KEILHACKER, M. and the JET TEAM, 'High Fusion Performance from Deuterium-Tritium Plasmas in the JET Tokamak', to be published in Nucl. Fusion.
[21] JACQUINOT, J. and the JET TEAM, 'Overview of ITER Physics Deuterium-Tritium Experiments in JET', to be published in Nucl. Fusion.
[22] LINGERTAT, J. et al., 'The Edge Operational Space in JET', Proc. 13th International Conf. On Plasma Physics Surface Interaction in Controlled Fusion Devices, San Diego, May 1998, to be published in J. Nucl Materials.
[23] JET TEAM, Progress Report 1996, JET Joint Undertaking, Abingdon (UK).
[24] KAYE, A. et al., Fusion Engineering and Design 24 (1994) 1.
[25] ORLINSKIJ, D.V. , MAGYAR, G., Nucl. Fusion 28 (1988) 611.
[26] JARVIS, N. et. al., Proc. 25th EPS Conf. on Plasma Physics, Prague, 1998, part I, 46.
[27] VON HELLERMANN, M. G. et al. in Diagnostics for Experimental Thermonuclear Fusion Reactors, Plenum Press, New York and London (1996) p. 281.
[28] ITER CONFINEMENT DATABASE AND MODELLING WORKING GROUP (Presented by J.G. CORDEY), Plasma Physics Controlled Fusion 39 supplement 12B (1997) B115.
[29] ERIKSSON, L-G. et al, Nucl. Fusion 33 (1993) 1037.
[30] POGUSTE, O. et al., in Controlled Fusion and Plasma Physics (Proc. 22nd Eur. Conf, Bournemouth, 1995), vol.19C, Part III, European Physical Society, Geneva (1995) 277.
[31] ITOH, S-I. et al, Plasma Physics Controlled Fusion, 38 (1996) 527.
[32] KAUFMAN, M. et al., in Fusion Energy (Proc.16th Int. Conf. Montreal, 1996), vol.1, IAEA, Vienna (1997) 79.
[33] LOARTE, A. et al., Plasma Physics 38 (1998) 11.
[34] IGITKHANOV, Yu et al., Plasma Physics 38 (1998) 73.
[35] KASS, T. at al., Nucl. Fusion, 38 (1998) 111.
[36] ROMANELLI, F., ZONCA, F., Phys. Fluids B, 5 (1993) 4081.
[37] JANESCHITZ, G. et al., in Controlled Fusion and Plasma Physics (Proc. 24th Eur. Conf, Berchtesgaden, 1997), vol.21A, Part III, European Physical Society, Geneva (1997) 993.
[38] SAIBENE, G., et. al., Proc. 25th EPS Conf. on Plasma Physics, Prague, 1998, part I, 33.
[39] POGUTSE, O. P, YURCHENKO, E., Rev. of Plasma Physics, 11 (1986) 65.
[40] HIROSE, A. et al. "Kinetic ballooning modes in tokamaks" Report Plasma Physics Laboratory, University of Saskatchewan, PPL-159, June 1996.
[41] SHAING K.C., CRUME Jr, E.C., Phys. Rev. Lett,. 63 (1989) 2369.
[42] WILSON, H.R., CONNOR, J.W., in Controlled Fusion and Plasma Physics (Proc. 24th Eur. Conf, Berchtesgaden, 1997), vol.21A, Part I, European Physical Society, Geneva (1997) 289.
[43] HINTON, F.L., STAEBLER, G.M., Phys. Fluids 5 (1993) 1281.

[44] GUO, H.Y., et. al. “Edge Transport Barrier in JET Hot-Ion H-Modes”, submitted for publication to Nucl. Fusion special issue.

[45] SAIBENE, G., et. a. “The Influence of Isotope Mass, Edge Magnetic Shear and Input Power on High Density ELMy H-Modes in JET”, submitted for publication in Nucl. Fusion.

[46] CORDEY, J. G. “H-mode Power Threshold and Confinement in JET H, D, D-T and T Plasmas” 17th IAEA Fusion Energy Conference, Yokohama 1998, paper IAEA-F1-CN69/ Ex7/1.

[47] PARAIL, V., Private communication, JET Joint Undertaking, 1998.

[48] ERIKSSON, L-G. et al, Phys Rev. Lett. 81 (1998) 1231.

[49] ITER CENTRAL TEAM, Final Design Report, International Thermonuclear Experimental Reactor Engineering Design Activity, San Diego Joint Work Site, La Jolla, California, 1997 (unpublished).